Date of publication xxxx 00, 0000, date of current version xxxx 00, 0000.

Digital Object Identifier 10.1109/ACCESS.2017.DOI

Low-Loss Periodically Air-Filled Substrate Integrated Waveguide (SIW) Band-Pass Filters

RAÚL GARCÍA[1], ÁNGELA COVES[1], (Senior Member, IEEE), DARÍO HERRAIZ[2], ÁNGEL A. SAN-BLAS[1], and MAURIZIO BOZZI[3], (Fellow, IEEE)

[1]Departamento de Ingeniería de Comunicaciones-I3E, Universidad Miguel Hernández de Elche, 03202 Elche, Spain
[2]Departamento de Igeniería Eléctrica, Electrónica, Automática y Comunicaciones, Universidad de Castilla-La Mancha, Escuela Politécnica de Cuenca, Campus Universitario, 16071 Cuenca, Spain)

[3]Department of Electrical, Computer and Biomedical Engineering, University of Pavia, Italy

Corresponding author: Ángela Coves (e-mail: angela.coves@umh.es).

This work has been funded in part by Ministerio de Ciencia e Innovación MCIN/AEI, and in part by Conselleria de Educación, Universidades y Empleo, Generalitat Valenciana under Project CIAICO/2021/055.

ABSTRACT The electrical response of low-frequency band-pass filters based on periodic substrate integrated waveguide (SIW) technology typically shows permitted and forbidden frequency bands. Therefore, this type of filters can be designed using a conceptually very simple and efficient procedure based exclusively on the study of the dispersion properties of the periodic structure. In this paper, we go a step further with the design of a periodically air-filled SIW band-pass filter in which part of the dielectric substrate is removed to reduce insertion losses, and whose unit cell parameters, which are directly related to the center frequency (f_c) and bandwidth (BW) of the first passband, and also to the first stopband or bandgap (BG) of the structure, have been appropriately selected for filtering purposes, thus providing some useful design rules. Furthermore, we apply the concept of glide symmetry for achieving a much larger fractional bandwidth (FBW) than that obtained in conventional air-filled SIW filters found in the technical literature. Finite implementations of both periodic structures with and without glide symmetry have been analyzed, showing their filtering response for validation purposes. Additionally, to overcome the matching level restrictions in the resulting air-filled periodic SIWs, a microstrip-to-SIW transition including a novel coupling iris is proposed. A prototype of the proposed air-filled glide-symmetric periodic SIW filter has been manufactured and experimentally validated, illustrating the potential of this technique to obtain large FBWs that can not be achieved in conventional air-filled SIW filters. The proposed filter proves to be a good candidate for millimeter wave applications.

INDEX TERMS Band-pass filters, substrate integrated waveguide (SIW), glide symmetry, microstrip transition.

I. INTRODUCTION

Band-pass filters are key elements in many microwave applications that must be integrated with other components of a communications system. In this regard, substrate integrated circuits (SICs) are good candidates for such applications, given their reduced sizes and weights with respect to the classical waveguide technology, and exhibiting higher quality factors than printed technology. Among the different SIC structures [1]– [5], the substrate integrated waveguides (SIWs) are the most popular, due to an easy manufacturing process, lower costs, and ease of integration with other planar circuits, antennas, and passive and active devices on the same substrate [6]– [12].

Recently, several modified SIWs have been proposed in which the dielectric substrate has been partially or fully removed to improve the quality factor [13]– [18], due to the reduction of the dielectric losses. Different implementations of such modified SIWs can be found in the technical literature, known as modified SIW (MSIW) [13], hollow SIW (HSIW) [14], air-filled SIW (AFSIW) [15], [19], dielectricless SIW (DSIW) [17] and empty SIW (ESIW) [18]. Such modified SIWs have been successfully used to implement

band-pass filters with diverse topologies and using different elements. Among them, it is worth mentioning the solutions based on considering inductive posts along the AFSIW [15], the use of perforated sections along the SIW as immitance inverters [20], the insertion of inductive coupled cavities [21], [22] and broadside coupled resonators [23], an strategy based on alternating line sections with and without dielectric materials [24], or a implementation based on inserting dielectric elements in an ESIW acting as dielectric resonators or impedance inverters [25].

Most of these band-pass filters based on AFSIWs and designed using different strategies, show narrow-band characteristics, having a fractional bandwidth around 3%. There are a few filter designs with higher FBWs, like an AFSIW design in [21], where FBW $= 15\%$, or the AFSIW band-pass filters presented in [20], [26] which present similar FBWs, but exhibit a poorer rejection band. Only an ESIW design, presented in [25], achieved an extremely large FBW of 31.5%, although the passband was too close to the ESIW cut-off frequency, and a poor matching was obtained in the lower passband edge, thus reducing substantially such value in practice. In [27], a higher symmetry called glide symmetry, which is created with a combination of a translation and mirroring over a plane, was applied to the design of a wide-band sub-wavelength CSRR-loaded SIW filter with FBW $= 26\%$, thus illustrating the potential of this technique to widen the passband of conventional SIW filters. However, a poor matching was again observed in the lower passband edge when using conventional taper transitions from microstrip to SIW. Besides, such design did not exhibit the low insertion losses of AFSIWs.

In this contribution, therefore, we take advantage of both the low insertion losses of AFSIWs and the passband broadening effect of glide symmetry with the aim of designing advanced band-pass filters in SIW technology exhibiting high values for the FBW. This is, in fact, the main objective of this work. To this end, we make use of the results obtained in a previous work of the authors [28], where, similarly, the dispersion characteristics of waves propagating in periodic SIWs with different periodic configurations (with and without glide symmetry) were used to achieve a significant broadening of the first passband when glide symmetry was considered in the structure. However, in the aforementioned work, less attention was paid to both the achieved matching level in the passband and to the obtained rejection bands. In this new contribution, we go a step further with the objective of achieving enhanced filtering electrical responses. To this aim, we first start with the design of a band-pass filter based on a periodic SIW structure partially filled with air, in order to benefit from low insertion losses due to the removal of dielectric material. In addition, we will provide useful design guidelines that can be used to meet the prescribed filter electrical specifications. In particular, the dispersion diagram of a design example of a periodic SIW with band-pass filtering characteristics associated to the existence of permitted and forbidden frequency bands is firstly presented. Additionally, some design curves are provided, from which appropriate unit cell parameters can be easily selected for achieving the desired filter center frequency and bandwidth. It will be shown that, starting from this initial filter, the introduction of glide symmetry can lead to an enhanced filter performance with a significant broadening of the first passband of the periodic structure, while keeping a wide rejection band at the same time (and also benefiting from low insertion losses due to the removal of dielectric material). Additionally, in order to improve the microstrip-to-SIW transition and overcome the matching level restrictions in the resulting air-filled periodic SIWs, a microstrip-to-SIW transition including a novel coupling iris is introduced, which was already proposed in ESIW technology [18].

It is worthwhile to emphasize at this point the main benefits of this filter design procedure with respect to alternative more traditional techniques. On the one hand, we want to point out the simplicity and efficiency (in terms of computation time) of this design procedure, which is based exclusively on the study of the dispersion properties of the periodic structure. These dispersion properties are directly related to the set of dimensions that define the unit cell, so they can provide us with useful design guidelines for getting the desired f_c and BW. On the other hand, as it will be shown aftwerwards, the obtained FBW in the proposed glide-symmetric filter has not been achieved in conventional air-filled SIW filters found in the technical literature, to the best of the authors' knowledge.

The paper is organized as follows. Section II presents the unit cell of the air-filled periodic SIW in the proposed initial filter design. Afterwards, its dispersion properties are rigorously described in terms of permitted and forbidden bands as a function of the unit cell parameters, including design guidelines for obtaining different values for f_c, BW and the first bandgap of the structure. Section III reports the great bandwidth increase that can be achieved when a glide symmetry is considered in the previously analyzed unit cell, and several design curves are also provided for filtering design purposes. In Section IV, we present several examples of finite implementations of the periodic geometries obtained in Sections II and III acting as band-pass filters, and the differences in their electrical response (mainly, in terms of FBW) are also emphasized. Additionally, a novel microstrip-to-SIW transition including a coupling iris is described for improving their matching level. A prototype of the obtained glide-symmetric periodic SIW filter, exhibiting a measured FBW equal to 36%, has been successfully fabricated and measured for validating purposes. Finally, a summary of our main conclusions is reported in Section V.

II. DISPERSION AND FILTERING PROPERTIES OF NON-GLIDE AIR-FILLED PERIODIC SIWS

Fig. 1(a) shows the scheme of the air-filled periodic SIW in the proposed initial filter design, which consists of a SIW of width a_{SIW}, whose lateral waveguide walls are delimited by vias characterized by their diameter $d_v = 0.8$ mm and

separation $s_v = 1.2$ mm, which have been appropriately chosen in order to avoid radiation losses [3] so they fulfill the following conditions:

$$d_v < \lambda_g/5, \qquad s_v \leq 2d_v \tag{1}$$

where λ_g is the guided wavelength. The propagation constant of this guide is determined by the width a_{SIW} of the SIW (see Fig. 1(a)), and also by the effective permittivity ϵ_{reff} obtained after periodically removing substrate material in the propagation area in order to create permitted and forbidden bands. Additionally, a decrease of the dielectric losses is expected due to the removal of material, which is an interesting feature in filter design. A previous study [3] demonstrates that a SIW can be analyzed as an equivalent rectangular waveguide of effective width a_{eff} given by:

$$a_{\text{eff}} = a_{SIW} - \frac{d_v^2}{0,95 s_v} \tag{2}$$

Therefore, all the study performed in this section is carried out using the equivalent waveguide of width a_{eff} given by eq. (2), and height b. In order to compare the dispersion characteristics of the structures under analysis, the parameters of the basis SIW waveguide have been set to the following values: width a_{SIW} = 23 mm, height of 0.63 mm (referred to the z-axis depicted in Fig. 1) and relative permittivity of the substrate equal to 10. The different parameters of the periodic structure (the period p and the parameters t_1 and t_2 in the studied periodic configuration) will determine the bandwidth and location of the different permitted and forbidden bands, which has been extensively analyzed in the technical literature [29]. It is important to mention that, as a consequence of the linearity of the field equations, the results can be directly scaled to any desired frequency range. In this section, we analyze the dispersion properties of the unit cell of Fig. 1(b) of period p with the commercial software tool Ansys HFSS, which is based on the Finite Element Method [30]. The eigenmode module of such analysis tool yields the resonance frequencies of the different propagative modes in the analyzed periodic cell with such parameters as a function of the phase delay, $\phi = \beta p$, between its periodicity planes, thus being β the modal phase constant of each propagative mode at such resonant frequencies. Alternative methodologies for calculating the dispersion diagram of the modes of periodic waveguides have been presented in [31]– [35].

In Fig. 2 it is represented the dispersion diagram of the first two modes (the first mode with black line and the second mode with blue line) of the periodic SIW shown in Fig. 1(b) with parameters $p = 23$ mm, $t_1 = 9.5$ mm and $t_2 = 7.5$ mm. This initial configuration will be referred in the following as Reference Case (with reference parameters: $p_{ref} = 23$ mm, $t_{1ref} = 9.5$ mm and $t_{2ref} = 7.5$ mm). The first passband of this initial periodic structure (corresponding to mode 1) extends from $f_1 = 3.23$ to $f_2 = 3.83$ GHz, being the center

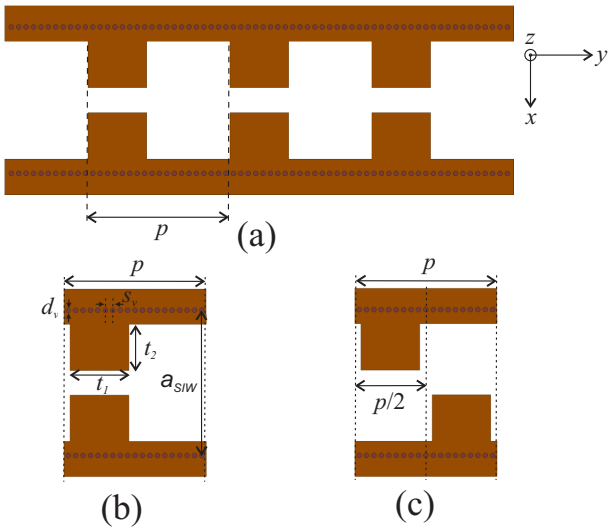

FIGURE 1. (a) Scheme of the proposed periodic SIW partially filled with air. (b) Unit cell of the initial periodic configuration (named non-glide configuration). (c) Unit cell of the same structure shown in case (b) when glide symmetry is applied.

frequency $f_c = 3.53$ GHz, and its bandwidth $\text{BW} = 0.6$ GHz, providing a significantly high $\text{FBW} = 17\%$, defined as:

$$\text{FBW} = \frac{f_2 - f_1}{f_c} \tag{3}$$

We can check that this mode is a TE_{10}-like mode, at the sight of the electric field distribution of such mode within the unit cell represented in Fig. 3(a) (which has been calculated at 3.23 GHz). This mode will be excited through a standard excitation at the center of the waveguide, like with an SMA connector connected to a microstrip-to-SIW transition. Next, a first stopband appears for mode 1 (marked in Fig. 2 with light blue colour) extending up to 6.2 GHz. Although mode 2 begins to propagate at a frequency (5.05 GHz) which falls within this stopband, the nature of mode 2 is a TE_{20}-like mode (as can be checked by its electric field distribution represented in Fig. 3(b) at this frequency), so it will not be excited using a standard excitation. In this regard, note that the electric field distribution related to this second mode shows that the electric field is cancelled at the center of the structure (at the $x = a_{SIW}/2$ plane), so we will be able to avoid its excitation, as it will be shown later in Section IV. Thus, this periodic SIW will have an effective rejection bandwidth (or bandgap, BG) of $\text{BG} = 2.37$ GHz. These will be the filter parameters obtained when using such unit cell in a filter design, as will be shown in Section IV.

Next, going a step further, and with the purpose of providing some design rules for filtering applications, we have represented in Fig. 4 the center frequency f_c of the first passband of mode 1 of this periodic SIW obtained from the analysis of the dispersion diagram with $t_2 = t_{2ref} = 7.5$ mm as a function of t_1, and for different values of the period p, where each period is expressed in terms of a scale factor f relative to the value of the reference period $p = p_{ref} = 23$ mm

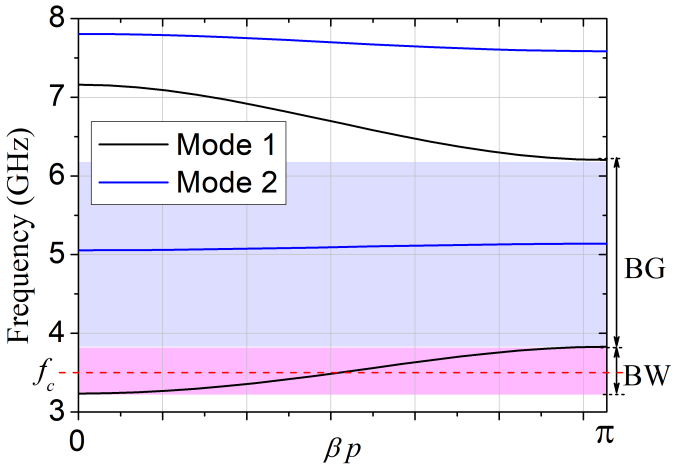

FIGURE 2. Dispersion diagram of the first two modes of the periodic SIW shown in Fig. 1(b) with the following parameters: $p = 23$ mm, $t_1 = 9.5$ mm and $t_2 = 7.5$ mm (parameters corresponding to the so-called Reference Case).

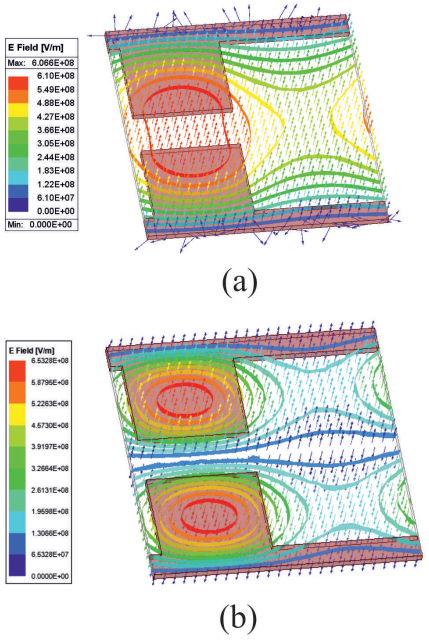

FIGURE 3. Electric field distribution within the unit cell of the periodic SIW shown in Fig. 1(b) with parameters corresponding to the Reference Case in Fig. 2. (a) Electric field distribution of mode 1 calculated at 3.23 GHz. (b) Electric field distribution of mode 2 calculated at 5.05 GHz.

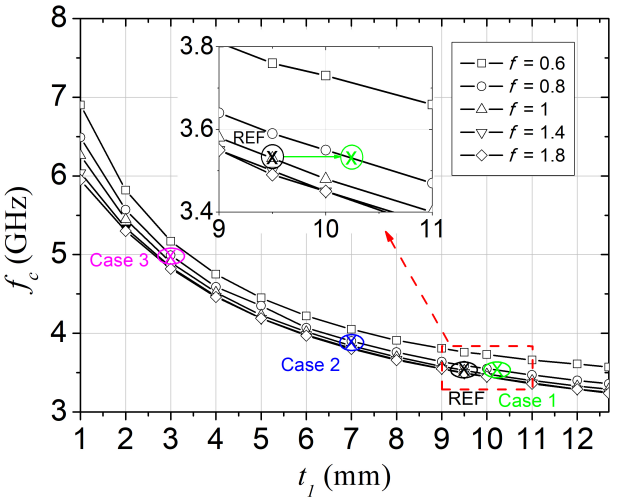

FIGURE 4. Variation of the center frequency (f_c) of the first passband of mode 1 as a function of t_1 ($t_2 = t_{2ref} = 7.5$ mm), obtained from the analysis of the dispersion diagram of the periodic SIW shown in Fig. 1(b). Different values of the scale factor f have been considered (f represents a scale factor of the reference period $p_{ref} = 23$ mm used in Fig. 2, i.e., $p = f \cdot p_{ref}$).

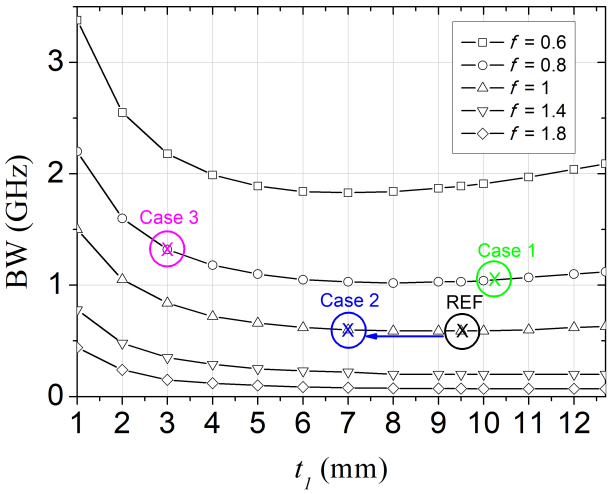

FIGURE 5. Variation of the bandwidth (BW) of the first passband of mode 1 of the periodic SIW shown in Fig. 1(b) as a function of t_1 ($t_2 = t_{2ref} = 7.5$ mm), and for different values of the period factor f.

used in Fig. 2, i.e., $p = f \cdot p_{ref}$. In the same way, Figs. 5 and 6 show the BW and BG of this periodic SIW obtained from its dispersion diagram with $t_2 = t_{2ref} = 7.5$ mm as a function of t_1 for different values of the period factor f. In these figures, the obtained filter parameters for the Reference Case defined in Fig. 2 have been highlighted with a black circle and named as REF. Thus, these tree figures can be conveniently used as practical tools to search the appropriate periodic SIW parameters for achieving a desired filter response in terms of f_c, BW and rejection band or BG.

Three additional examples of filter design parameters based on this periodic structure have been highlighted in Figs. 4-6 in order to show how to use the information provided in such figures. In the first one, labelled as Case 1, f_c has been fixed but a higher BW has been obtained, for which we have moved along an horizontal line of constant f_c in Fig. 4 from the initial point (REF) to the right until the point marked with a green circle named Case 1 (see the zoom in the figure inset), cutting the curve with period factor $f = 0.8$ at $t_1 = 10.23$ mm. With these new values of f and t_1, we can read in Fig. 5

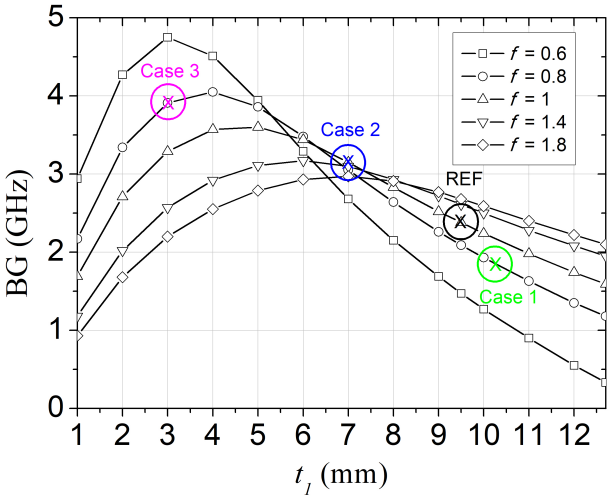

FIGURE 6. Variation of the first bandgap (BG) of mode 1 of the periodic SIW shown in Fig. 1(b) as a function of t_1 ($t_2 = t_{2ref} = 7.5$ mm), and for different values of the period factor f.

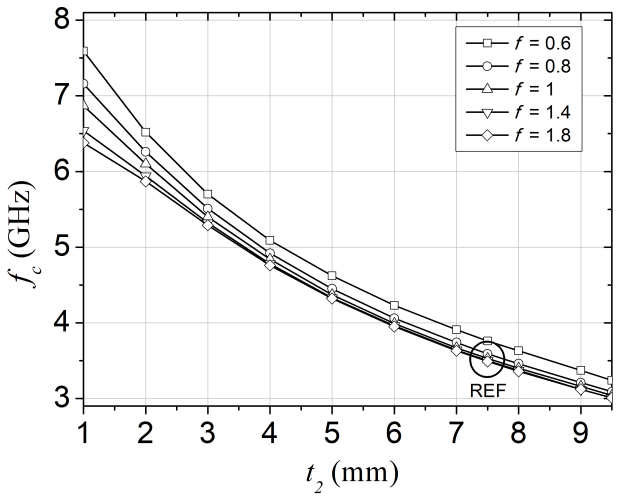

FIGURE 7. Variation of the center frequency (f_c) of the first passband of mode 1 of the periodic SIW shown in Fig. 1(b) as a function of t_2 ($t_1 = t_{1ref} = 9.5$ mm), and for different values of the period factor f.

a new (higher in this case) BW $= 1.05$ GHz (marked again as Case 1 with a green circle in this figure). These modified parameters will provide a lower BG $= 1.85$ GHz in Case 1, marked in Fig. 6 with a green circle.

Unlike Case 1, in Case 2 we have maintained the BW of the Reference Case, but we have chosen a different f_c (higher in this case), following this design process: we have moved along an horizontal line of constant BW in Fig. 5 from the initial point (REF) to the left until the point marked with a blue circle labelled as Case 2, which is placed on the curve of the same period factor $f = 1$ but at a new value of $t_1 = 7$ mm, which yields a higher $f_c = 3.84$ GHz at the sight of Fig. 4. Similarly to the previous case, the new parameter t_1 provides a different value of BG, as can be seen in Fig. 6, which has moved from the initial value of 2.37 GHz (black circle, REF case) to a higher value of 3.15 GHz (blue circle, Case 2).

A third example of filter design can be followed making use of the information provided through the parameter sweep of t_1 shown in Figs. 4-6, labelled as Case 3 and marked with a pink circle. In this new example, different values of f_c and BW have been obtained from those derived in the Reference Case (both higher in this case), which have been obtained in this example by selecting the parameters $f = 0.8$ and $t_1 = 3$ mm. Such higher values of f_c and BW can be explained as follows: on the one hand, a lower value of $f = 0.8$ (lower period) instead of the value $f = 1$ for the Reference Case implies a lower consecutive distance between the high dielectric permittivity regions in the periodic waveguide where the fields of mode 1 mostly concentrate as seen in Fig. 3(a), and thus there is a higher coupling between such fields, resulting in a higher BW of the passband. On the other hand, a lower value of $t_1 = 3$ mm instead of $t_1 = 9.5$ mm results in a lower mean value of the effective permittivity in the unit cell, resulting in a higher passband of mode 1 (which 'sees' a lower mean effective permittivity), and consequently, in a higher center frequency f_c of such passband. At the sight of Fig. 4, the new f_c is equal to 5.0 GHz (instead of 3.53 GHz), while Fig. 5 shows that the new BW is of 1.32 GHz (instead of 0.6 GHz), being the resulting BG equal to 3.91 GHz instead of 2.37 GHz (see the pink circle labelled as Case 3 in Fig. 6). Thus, we can conclude that Figs. 4-6 can be easily employed to get the desired filter design specifications in terms of f_c, BW and BG, which will be somehow restricted by the possible values of the waveguide parameters (f, t_1 and t_2). In particular, t_1 must be always lower than the period $p = f \cdot p_{ref}$, and t_2 must be lower than $a_{SIW}/2$.

Previously, in Figs. 4-6, the parameter t_2 has been fixed to 7.5 mm, while t_1 has been swept from 1 to 12.7 mm. Alternatively, an additional degree of freedom can be achieved in the filter design previously described when using the periodic SIW shown in Fig. 1(b) if the parameter t_2 is varied. Figs. 7-9 yield different filter parameters (f_c, BW and BG) when t_1 is fixed to 9.5 mm (corresponding to the Reference Case) and a parametric sweep of t_2 is performed from 1 to 9.5 mm for several values of the period factor f. Thus, different values of f_c, BW and BG from those obtained in the Reference Case (marked in such figures with a black circle and labelled as REF) can be properly achieved with a similar analysis to the one previously described.

Finally, in this unit cell configuration, it has been shown that appropriate unit cell parameters can be selected to achieve a desired BW by either using Figs. 4-6 or Figs. 7-9. However, the obtained BWs are rather low (mainly lower than 1.5 GHz). Although higher values of BW can be achieved for reduced periods (see the curves corresponding to $f = 0.6$ in Figs. 5 and 8), the obtained BG in Fig. 9 for $f = 0.6$ is lower than 1.5 GHz for all values of t_2. On the other hand, in Fig. 6 we can check that the BG for $f = 0.6$

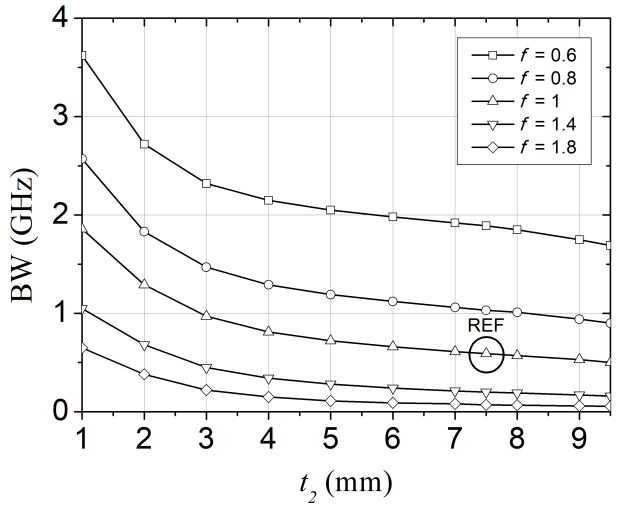

FIGURE 8. Variation of the bandwidth (BW) of the first passband of mode 1 of the periodic SIW shown in Fig. 1(b) as a function of t_2 ($t_1 = t_{1ref} = 9.5$ mm), and for different values of the period factor f.

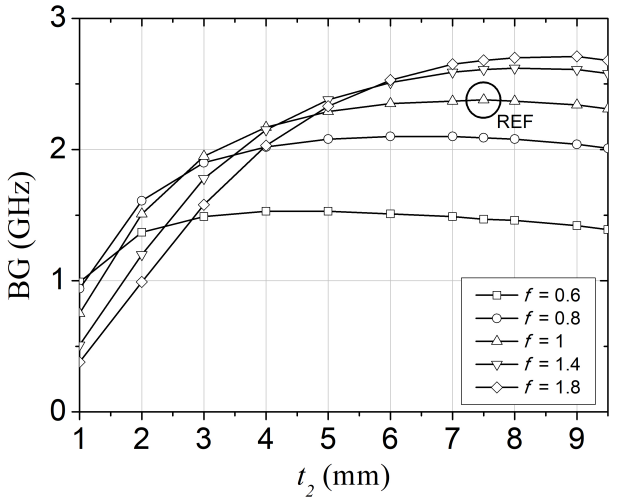

FIGURE 9. Variation of the first bandgap (BG) of the first passband of mode 1 of the periodic SIW shown in Fig. 1(b) as a function of t_2 (with $t_1 = t_{1ref} = 9.5$ mm), and for different values of the period factor f.

is also drastically reduced when increasing t_1 (BG < 2.0 GHz for $t_1 > 8.0$ mm), and consequently, it is not possible to achieve a high FBW without worsening the rejection band. Thus, in order to achieve an acceptable rejection band, t_1 must be low, and given that f_c increases rapidly when diminishing t_1, as seen in Fig. 4, the resulting FBW will be low. This aspect was already mentioned in the introduction section, i.e., the difficulty found in the technical literature for obtaining high FBWs with these filter topologies.

III. DISPERSION AND FILTERING PROPERTIES OF GLIDE-SYMMETRIC AIR-FILLED PERIODIC SIWS

If we want to achieve a band-pass filter response with higher FBW without reducing the rejection band with this same topology of periodic SIW, we can take advantage of the glide symmetry, by applying such symmetry over the periodic SIW shown in Fig. 1(b), as it can be seen in Fig. 1(c). The dispersion diagram of the first two modes of this new structure is represented in Fig. 10 for the Reference Case in the glide configuration (with parameters $p = 23$ mm, $t_1 = 9.5$ mm and $t_2 = 7.5$ mm), along with their electric field distribution represented in Fig. 11 at different frequencies.

The first passband of this glide-symmetric periodic structure (corresponding to mode 1) extends from 3.28 to 4.87 GHz, being the center frequency $f_c = 4.08$ GHz (see Fig. 10). In this way, as already shown in previous works [27], [28], the obtained glide-symmetric unit cell (with exactly the same parameters of the non-glide Reference Case) has nearly the same cutoff frequency (3.28 GHz instead of 3.23 GHz), but a much wider BW, that changes from 0.6 GHz in the non-glide configuration to 1.59 GHz in this case. Although the f_c has also moved from 3.53 GHz to 4.08 GHz, the resulting FBW increases from 17% to 39%, a much higher value compared to other AFSIW filters presented in the technical literature, to the knowledge of the authors. Besides, it is also interesting to note that, in this case, the resulting rejection band is still quite high (BG $= 2.09$ GHz) in this glide-symmetric configuration. In this regard, it is worth mentioning that, unlike the previously studied non-glide configuration of periodic SIW in Section II, the second mode in this glide-symmetric unit cell (labelled as Mode 2 and represented with blue line in Fig. 10) will delimit the end of the first rejection band since it will be excited with a standard excitation, given that it is not a TE_{20}-like mode in this case; i.e., the electric field is not cancelled at the $x = a_{SIW}/2$ plane, as can be checked in Fig. 11(b), where it is represented the electric field distribution of mode 2 at 7.19 GHz. Therefore, this periodic SIW will have an effective rejection bandwidth of BG $= 2.09$ GHz. These will be the filter parameters obtained when using such glide-symmetric unit cell in a filter design, as will be shown in Section IV.

Again, with the aim of providing some design rules for filter design purposes when using this topology of unit cell, we have represented in Fig. 12 the center frequency f_c of the first passband of mode 1 of this glide-symmetric periodic SIW, obtained from the analysis of the dispersion diagram. In particular, we have represented the variation of f_c as a function of t_1 (we have set $t_2 = t_{2ref} = 7.5$ mm), and for different values of the period factor f (relative to the value of the reference period $p = p_{ref} = 23$ mm used in Fig. 10, i.e., $p = f \cdot p_{ref}$). Similarly, Figs. 13 and 14 show the BW and BG of the glide-symmetric periodic SIW as a function of t_1 (we have set $t_2 = t_{2ref} = 7.5$ mm) for different values of the period factor f. In these figures, the obtained filter parameters for the Reference Case defined in Fig. 10 have been highlighted with a black circle and labelled as REF.

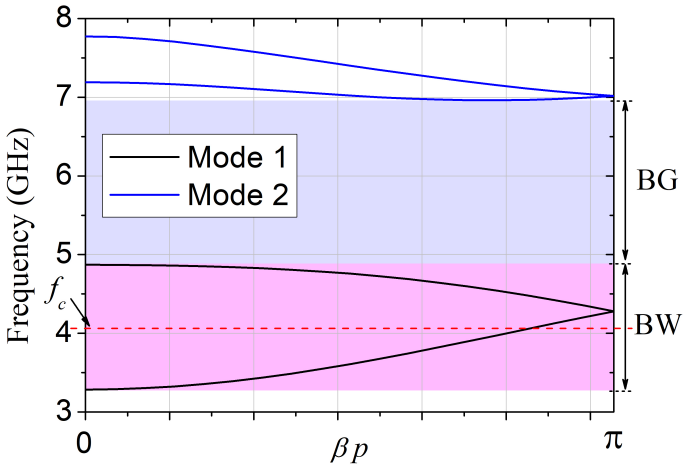

FIGURE 10. Dispersion diagram of the first two modes of the periodic SIW with glide symmetry shown in Fig. 1(c), with parameters $p = 23$ mm, $t_1 = 9.5$ mm and $t_2 = 7.5$ mm (corresponding to the Reference Case for the glide configuration).

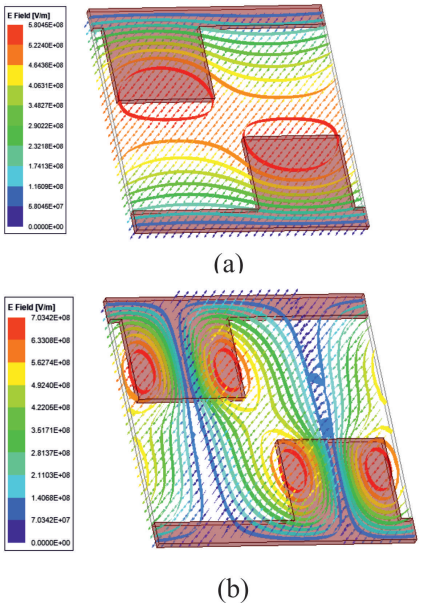

FIGURE 11. Electric field distribution within the unit cell of the glide-symmetric periodic SIW shown in Fig. 1(c), with parameters corresponding to the Reference Case for the glide configuration in Fig. 10. (a) Electric field distribution of mode 1 calculated at 3.28 GHz. (b) Electric field distribution of mode 2 calculated at 7.19 GHz.

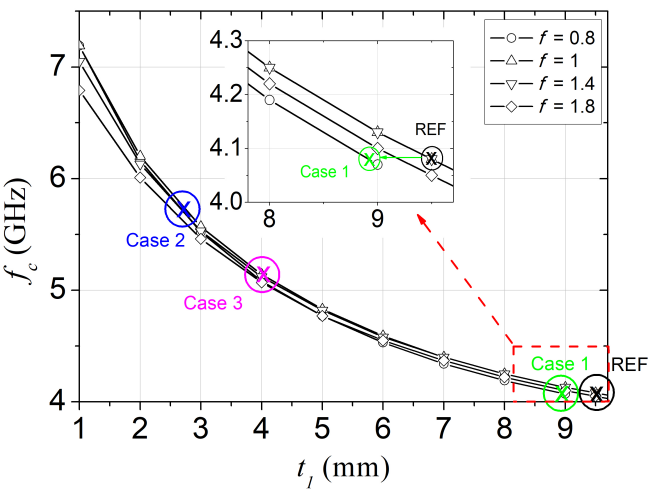

FIGURE 12. Variation of the center frequency (f_c) of the first passband of mode 1 of the glide-symmetric periodic SIW shown in Fig. 1(c) as a function of t_1 ($t_2 = t_{2ref} = 7.5$ mm), and for different values of the period factor f.

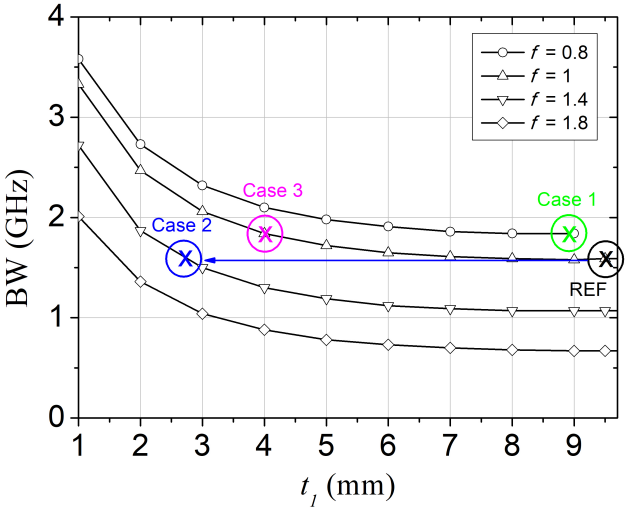

FIGURE 13. Variation of the bandwidth (BW) of the first passband of mode 1 of the glide-symmetric periodic SIW shown in Fig. 1(c) as a function of t_1 ($t_2 = t_{2ref} = 7.5$ mm), and for different values of the period factor f.

Thus, these three figures can be conveniently used as practical tools to search the appropriate glide-symmetric periodic SIW parameters for achieving a desired filter response in terms of f_c, BW and rejection band.

Next, we have analysed the same three cases studied in Section II, but for the glide-symmetric configuration. In this way, it can be compared the difference in the results provided by both configurations. Beginning with Case 1, we first set the value of f_c and obtain a higher value of BW. To this aim, we have moved along an horizontal line of constant f_c in Fig. 12 from the initial point (REF) to the left, cutting the curve with period factor $f = 0.8$ at $t_1 = 8.93$ mm (see the green circle labelled as Case 1 in the figure inset). With these new values of f and t_1, we can read in Fig. 13 the higher $\mathrm{BW} = 1.84$ GHz obtained (labelled again as Case 1 with a green circle in this figure), providing in this case an extremely high $\mathrm{FBW} = 45.1\%$, which has been obtained due to the introduction of glide-symmetry. In addition, these modified parameters will provide a higher $\mathrm{BG} = 2.14$ GHz for Case 1, marked in Fig. 14 with a green circle.

Unlike Case 1, if our design objective is keeping the reference BW and obtain a different f_c, the design process is

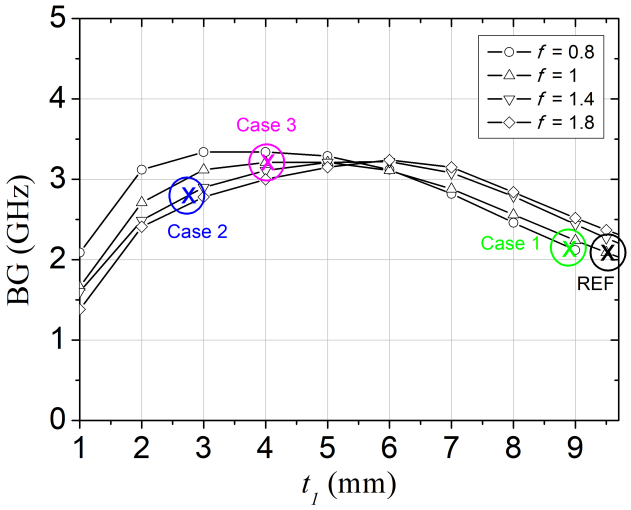

FIGURE 14. Variation of the first bandgap (BG) of the glide-symmetric periodic SIW shown in Fig. 1(c) as a function of t_1 ($t_2 = t_{2ref} = 7.5$ mm), and for different values of the period factor f.

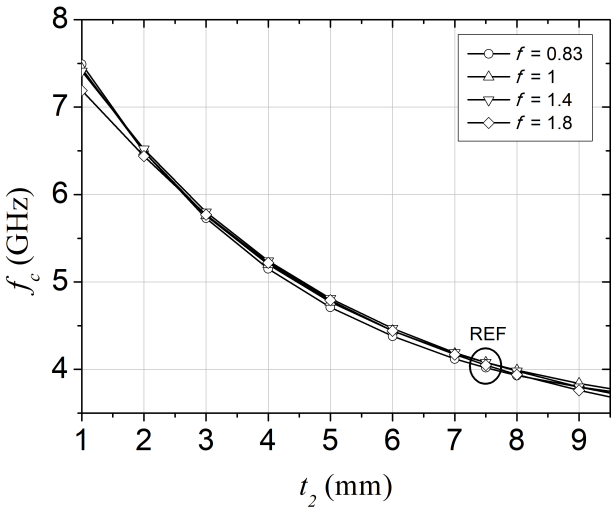

FIGURE 15. Variation of the center frequency (f_c) of the first passband of mode 1 of the glide-symmetric periodic SIW shown in Fig. 1(c) as a function of t_2 ($t_1 = t_{1ref} = 9.5$ mm), and for different values of the period factor f.

as follows: we can move along an horizontal line of constant BW in Fig. 13 from the initial point (REF) to the left until the point marked with a blue circle labelled as Case 2, which is placed on the curve of period factor $f = 1.4$ at a new value of $t_1 = 2.7$ mm, which yields a higher $f_c = 5.69$ GHz at the sight of Fig. 12. Similarly to the previous cases, the new parameters t_1 and f provide a different value of BG as can be seen in Fig. 14, which has moved from the initial value of 2.09 GHz (black circle, REF case) to a higher value of 2.81 GHz (blue circle, Case 2).

A third example of filter design has been followed making use of the information provided through the parameter sweep of t_1 shown in Figs. 12-14, labelled as Case 3 and marked with a pink circle, which consists of getting different values of f_c and BW from those obtained in the Reference Case (both higher in this case). To this aim, we have selected the parameters $f = 1$ and $t_1 = 4$ mm. At the sight of Fig. 12, the new value of f_c is equal to 5.14 GHz (instead of 4.08 GHz), while Fig. 13 shows that the new value of BW is equal to 1.84 GHz (instead of 1.59 GHz). Moreover, the resulting BG is now of 3.21 GHz (see the pink circle labelled as Case 3 in Fig. 14). Thus, we can conclude that Figs. 12-14 can be easily employed to get the desired filter design specifications in terms of f_c, BW and BG, which will be somehow restricted by the possible values of the waveguide parameters (f, t_1 and t_2). In particular, t_1 must be always lower than the period $p = f \cdot p_{ref}$, and t_2 must be lower than $a_{SIW}/2$.

Previously, in Figs. 12-14, the parameter t_2 has been fixed to 7.5 mm, while t_1 has been swept from 1 to 9.5 mm. Again, an additional degree of freedom can be achieved in the filter design previously described when using the periodic SIW shown in Fig. 1(c) if the parameter t_2 is varied. Figs. 15-17 yield different filter parameters (f_c, BW and BG) when t_1 is set to 9.5 mm (corresponding to the Reference Case) and

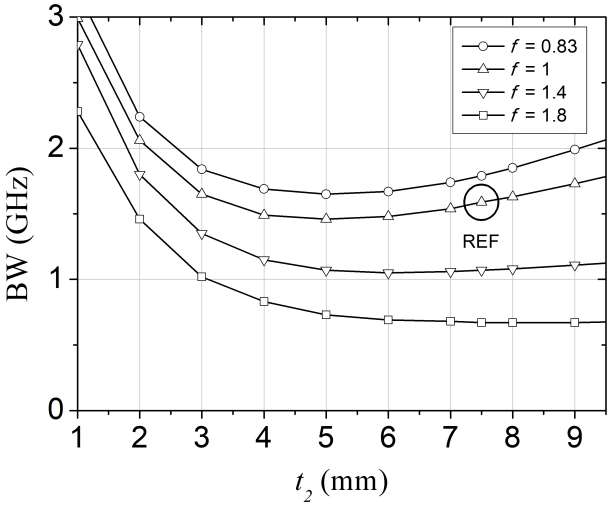

FIGURE 16. Variation of the bandwidth (BW) of the first passband of mode 1 of the glide-symmetric periodic SIW shown in Fig. 1(c) as a function of t_2 ($t_1 = t_{1ref} = 9.5$ mm), and for different values of the period factor f.

a parametric sweep is performed on t_2 from 1 to 9.5 mm for several values of the period factor f. Thus, different values of f_c, BW and BG from those obtained in the Reference Case (marked in such figures with a black circle and labelled as REF) can be properly achieved with a similar analysis to the one previously described.

IV. FINITE IMPLEMENTATIONS OF AIR-FILLED PERIODIC SIWS ACTING AS BAND-PASS FILTERS

The dispersion behaviour of air-filled periodic SIWs described in the previous sections showed their property to generate passbands and stopbands, and thus, their suitability to design band-pass filters with the desired specifications

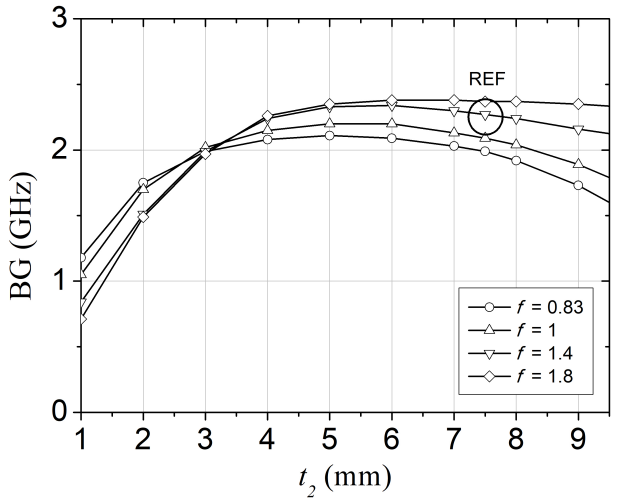

FIGURE 17. Variation of the band-gap (BG) of the first passband of mode 1 of the glide-symmetric periodic SIW shown in Fig. 1(c) as a function of t_2 ($t_1 = t_{1ref} = 9.5$ mm), and for different values of the period factor f.

in terms of f_c, BW and BG by properly selecting the unit cell parameters. As a proof of concept, in this section we present two filter designs based on finite implementations of both the conventional and glide-symmetric periodic configurations studied in Sections II and III, respectively. The number of periodic cells in the finite implementation of air-filled periodic SIWs acting as band-pass filters is directly related to the depth of the obtained rejection band, i.e., a higher number of periodic cells yields a deeper rejection band. In both cases, only 3 unit cells have proven to be enough to achieve a sufficiently deep rejection band, as will be shown later.

Fig. 18 shows the scheme of a first band-pass filter composed of 3 unit cells of the non-glide air-filled periodic SIW named as Reference Case in Section II (whose parameters are $p = p_{ref} = 23$ mm, $t_1 = t_{1ref} = 9.5$ mm and $t_2 = t_{2ref} = 7.5$ mm). The values of f_c, BW and BG related to this structure were determined by the dispersion diagram of such unit cell. The size of the first and last air boxes denoted by $l_a = 9.75$ mm (see Fig. 18) has been optimized in order to improve the electrical performance of the final filter. Regarding the microstrip line, note that the strip width has been fixed to $w_m = 0.6$ mm in order to provide a $Z_0 = 50\,\Omega$ impedance in this substrate, while the total length occupied by the taper plus the microstrip line has been fixed to $l_m = 13$ mm (see Fig. 18). On the other hand, with the aim of achieving a good return loss level in the passband, the modal impedance of the periodic air-filled SIW needs to be matched to that of the excitation microstrip line. To this end, a standard tapered transition has been employed, whose dimensions w_t and l_t (see Fig. 18) have been optimized. In the optimization process, we used the Quasi Newton (Gradient) Optimizer provided by Ansys HFSS commercial software. The optimized variables were the width and length of the taper, and

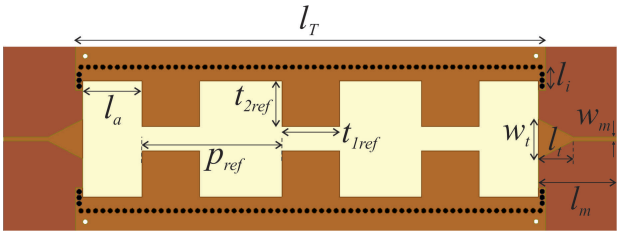

FIGURE 18. Scheme of a band-pass filter based on the unit cell depicted in Fig. 1(b) consisting of a non-glide air-filled periodic SIW named as Reference Case in Section II.

we selected as cost function the S_{11} (dB) parameter to be lower than -15 dB in the passband.

To further improve the obtained matching level in both air-filled periodic SIW filters designed in this section (specially, in the glide-symmetric filter with a high BW designed afterwards), a novel coupling iris has been introduced in the transition plane between the taper and the periodic SIW, as was already proposed in ESIW technology [18], with very good results. As can be seen in Fig. 18, the irises have been implemented with via holes using the same diameter d_v employed in the SIW walls. Moreover, the number of holes and their separation defining the iris width l_i have also been adjusted in a final optimization process. The obtained taper and iris dimensions for this first non-glide filter are $w_t = 6.51$ mm, $l_t = 5.74$ mm and $l_i = 3.53$ mm, thus achieving a filter whose total length (excluding the taper transitions and microstrip lines) is equal to $l_T = 77.4$ mm. Dielectric and conductor losses have been also considered in all simulations ($\tan\delta = 0.0035$ for the substrate material and $\sigma_{Cu} = 5.8{\cdot}10^7$ $\mathrm{S{\cdot}m^{-1}}$ for the metallization).

The simulated electrical response of this band-pass filter (obtained with Ansys HFSS) has been represented in Fig. 19. The passband, defined at a 10 dB input matching level, can be observed from 3.32 to 3.73 GHz (the analysis of the dispersion diagram predicted a passband from 3.23 to 3.83 GHz), yielding a FBW $= 12\%$. Despite having used only 3 periods, a deep rejection band which extends up to 6.26 GHz (6.2 GHz from the dispersion diagram) can be observed. Furthermore, we can check that mode 2 has not been excited, as expected. The obtained insertion losses are lower than 2 dB from 3.33 GHz to 3.72 GHz, being of 1.07 dB at the center frequency $f_c = 3.53$ GHz. Therefore, we can conclude that the electrical response of this filter fits perfectly the predicted one by the analysis of the dispersion diagram of the unit cell.

A second periodic band-pass filter with the alternative glide-symmetric configuration unit cell depicted in Fig. 1(c) has been designed and fabricated, by using 3 unit cells of the glide-symmetric air-filled periodic SIW named as Reference Case studied in Section III. The scheme of this filter is shown in Fig. 20(a). Again, the filter parameters f_c, BW and BG were determined by the dispersion diagram of such unit cell. In order to achieve a final design leading to a fair comparison in terms of insertion losses, the air-gap size $l_a = 4$ mm (see

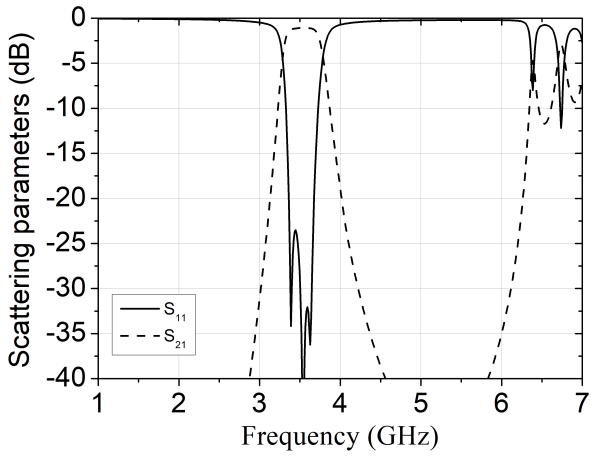

FIGURE 19. Simulated S-parameters of the non-glide air-filled periodic SIW filter of Fig. 18.

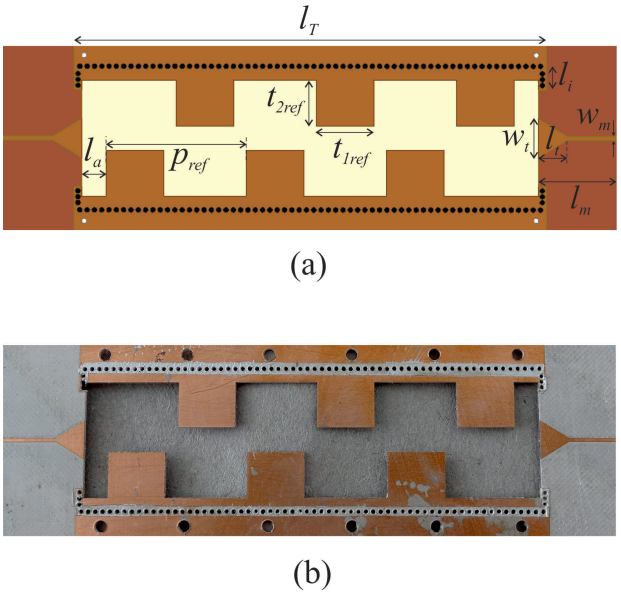

FIGURE 20. Band-pass filter based on the unit cell depicted in Fig. 1(c) consisting of a glide-symmetric air-filled periodic SIW named as Reference Case in Section II. (a) Scheme of the filter. (b) Photograph of the fabricated filter.

Fig. 20(a)) has been chosen in such a way that the total filter length $l_T = 77.4$ mm remains the same as in the previous design (the value of the strip width and the total length occupied by the taper plus the microstrip line have also been set as in the previous design; i.e., $w_m = 0.6$ mm and $l_m = 13$ mm). In this regard, it is also worth mentioning that l_a can be set to the desired value because, as already explained in Section III, the value of l_a is not critical in this glide-symmetric configuration since, although the excitation of the second mode of the periodic structure cannot be avoided, its cutoff frequency is far away from the filter passband.

After a final optimization process (using Ansys HFSS) on the taper and iris dimensions, the obtained values for this second filter with glide symmetry are $w_t = 6.41$ mm, $l_t = 4.73$ mm, and $l_i = 3.53$ mm. The simulated electrical response of this filter is represented in Fig. 21 using black lines. Regarding the obtained passband (which is defined at a 10 dB input matching level), it can be observed that it extends from 3.37 to 4.83 GHz (the analysis of the dispersion diagram predicted a passband from 3.28 to 4.87 GHz), and a deep rejection band which extends up to 7.0 GHz (6.96 GHz from the dispersion diagram), despite only 3 periods have been used. The obtained insertion losses are lower than 2 dB from 3.35 GHz to 4.76 GHz, being the insertion loss of 1.18 dB at the center frequency $f_c = 4.1$ GHz. Once again, the simulated electrical response of this filter fits perfectly the predicted one by the analysis of the dispersion diagram of the unit cell.

This glide-symmetric filter has been fabricated using a dielectric substrate Taconic CER-10, with a thickness of 0.63 mm, relative dielectric permittivity of $\varepsilon_r = 10$, loss tangent $\tan\delta = 0.0035$, and metal conductivity $\sigma = 5.8 \cdot 10^7$ S/m. An LPKF milling machine was adopted to pattern the metal layers and to drill the holes through the substrate, and conductive paste was used to metallize the via holes of the side walls. A photograph of the prototype is shown in Fig. 20(b). The air regions have been closed by copper tape on both sides (not shown in the photograph), to avoid any radiation leakage. A more standard manufacturing process could be the one adopted in [21], based on multilayered printed-circuit board technology. The fabricated prototype has been experimentally characterized, and several measurements were performed in the frequency band from 1 to 8 GHz by using a Rohde & Schwarz ZNB20 Vector Network Analyzer. No deembedding was applied to the measured results, to remove the connectors and transitions effect. The measurements are represented with red lines in Fig. 21, showing a very good agreement with HFSS simulations. The small observed discrepancies may be attributed to the combined effect of dielectric permittivity variation, the fabrication inaccuracies (for instance, in the top/bottom metal plates), and the connector effects (which will mainly affect the insertion loss, causing the measured filter to have higher insertion loss than the simulated one). As a consequence, there is a very small shift in the measured f_c of the filter, while the BW remains the same, and the insertion loss is a bit higher. The observed frequency shift is more noticeable at high frequencies, where the upper rejection band limit has increased a bit more in the measurement than in the simulation. The measured BW, defined at a 10 dB input matching level, is of 1.52 GHz, while the measured f_c is equal to 4.26 GHz, therefore yielding a FBW $= 36\%$, which, to the best of the authors' knowledge, is the highest value achieved in band-pass filters based on AFSIWs. The measured insertion loss is equal to 1.8 dB at the center frequency, which includes connectors and transitions losses, compared to 1.18 dB in the simulation (which does not include the connector effects).

The electrical performance of the two band-pass filters

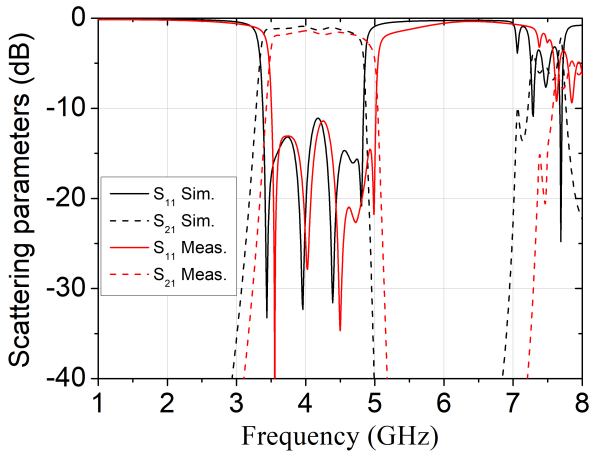

FIGURE 21. Simulated and measured S-parameters of the glide-symmetric air-filled periodic SIW filter of Fig. 20.

TABLE 1. Performance characteristics of the two designed air-filled periodic SIW filters compared to other similar filters found in the technical literature.

	f_c (GHz)	FBW (%)	Insertion loss at f_c (dB)	Return loss at f_c (dB)	Max. reject. depth (dB)
[21]	31.65	15.04	0.18	20	14
[26]	2.60	20	1.66	22	42
[20]	2.60	17.2	1.31	23	22
[25]	9.5	31.5	0.95	–	28
Fig. 19	3.53	12	1.07	35	>40
Fig. 21	4.26	36	1.8	12	>40

designed in this section are compared in Table 1 with other modified SIW band-pass filters with partially or fully removed substrate. Among the different designs, the proposed filters in this work show high FBWs (specially in the glide-symmetric case) along with very good insertion and return losses in the passband, as well as an extended rejection band. Such filters could be applied in satellite communication systems working at either S band (2-4 GHz) or C band (4-8 GHz) in miniaturized satellites (or smallsats) on low earth orbits (LEO) for data services or satellite TV networks.

V. CONCLUSION

In this work, a very simple and efficient filter design procedure is proposed to design band-pass filters based on air-filled periodic SIWs, both with and without glide symmetry. The proposed method is based on the analysis of the dispersion properties of the periodic structure, which are directly related to the dimensions defining the unit cell. Such dimensions can, therefore, be appropriately selected to meet the prescribed electrical specifications, so that several design curves can be readily obtained for filtering purposes. These design curves can be conveniently used as practical tools to search the appropriate periodic SIW parameters for achieving a desired filter response in terms of the filter center frequency, bandwidth and rejection band. Two band-pass filters based on the proposed air-filled periodic SIWs (with and without glide symmetry) have been designed, highlighting the differences in their electrical response mainly in terms of fractional bandwidth, as already evidenced by their respective dispersion diagrams. A prototype of a glide-symmetric band-pass filter with a high FBW has been fabricated and a very good agreement between simulated and experimental data has been observed, thus fully validating the proposed design procedure. Finally, although a prescribed matching level cannot be obtained in these air-filled periodic SIW filters, which can be seen as a drawback with respect to other conventional filtering designs, a microstrip-to-SIW transition including a novel coupling iris has proven to overcome the matching level restrictions. And most of all, it has been demonstrated the potential of this technique to obtain large FBWs (even higher than 40%) that have not been achieved in conventional air-filled SIW filters. As a future work, these filters can be designed at millimeter wave frequencies following the described design procedure, at which the removal of dielectric material will be more relevant.

REFERENCES

[1] K. Wu, D. Deslandes, and Y. Cassivi, "The substrate integrated circuits–A new concept for high-frequency electronics and optoelectronics," in *Proc. 6th Int. Conf. Telecommun. Modern Satell. Cable Broadcast. Service (TELSIKS)*, Nis, Yugoslavia, Vol. 1, pp. 3–10, Oct. 2003.

[2] D. Deslandes, M. Bozzi, P. Arcioni, and K. Wu, "Substrate integrated slab waveguide (SISW) for wideband microwave applications," in *IEEE MTT-S Int. Microw. Symp. Dig.*, Philadelphia, USA, pp. 1103–1106, Jun. 2003.

[3] Y. Cassivi and K. Wu, "Substrate integrated nonradiative dielectric waveguide," *IEEE Microw. Wireless Compon. Lett.*, Vol. 14, No. 3, pp. 89–91, Mar. 2004.

[4] F. Xu and K. Wu, "Guided-wave and leakage characteristics of substrate integrated waveguide," *IEEE Trans. Microw. Theory Techn.*, Vol. 53, No. 1, pp. 66–73, Jan. 2005.

[5] Q. Lai, C. Fumeaux, W. Hong, and R. Vahldieck, "Characterization of the propagation properties of the half-mode substrate integrated waveguide," *IEEE Trans. Microw. Theory Techn.*, Vol. 57, No. 8, pp. 1996–2004, Aug. 2009.

[6] M. Bozzi, A. Georgiadis, and K. Wu, "Review of substrate-integrated waveguide circuits and antennas," *IET Microw., Antennas Propag.*, Vol. 5, No. 8, pp. 909–920, Jun. 2011.

[7] Y. F. Tang, K. Wu, and N. K. Mallat, "Development of substrate-integrated waveguide filters for low-cost high-density RF and microwave circuit integration: Direct-coupled cavity bandpass filters with Chebyshev response," *IEEE Access*, Vol. 3, pp. 1313–1325, 2015.

[8] F. Grine, T. Djerafi, M. T. Benhabiles, K. Wu, and M. L. Riabi, "High-Q substrate integrated waveguide resonator filter with dielectric loading," *IEEE Access*, Vol. 5, pp. 12526–12532, 2017.

[9] L. Ye, Y. Chen, K. D. Xu, W. Li, Q. H. Liu, and Y. Zhang, "Substrate integrated plasmonic waveguide for microwave bandpass filter applications," *IEEE Access*, Vol. 7, pp. 75957–75964, 2019.

[10] S. Lee, S. Nam, and J. Lee, "Practical design and implementation method for asymmetric-response post-loaded substrate-integrated waveguide filters," *IEEE Access*, Vol. 8, pp. 101528–101538, 2020.

[11] Z. Xu, Y. Shi, C. Xu, and P. Wang, "A novel dual mode substrate integrated waveguide filter with mixed source-load coupling (Mslc)," *Progress In Electromagnetics Research*, Vol. 136, pp. 595–606, 2013.

[12] O. I. Hussein, K. A. A. Shamaileh, N. I. Dib, A. Nosrati, S. Abushamleh, D. G. Georgiev, and V. K. Devabhaktuni, "Substrate integrated waveguide bandpass filtering with Fourier-varying via-hole walling," *IEEE Access*, Vol. 8, pp. 139706-139714, 2020.

[13] L. Jin, R. M. A. Lee, and I. Robertson, "Reduction of dielectric losses in substrate integrated waveguide," *Electron. Lett.*, Vol. 42, No. 21, pp. 1230–1231, 2006.

[14] Q. Lai, C. Fumeaux, W. Hong, and R. Vahldieck, "Analysis and design of a novel lowloss hollow substrate integrated waveguide," *IEEE Trans. Microw. Theory Techn.*, Vol. 62, No. 8, pp. 1616–1624, Aug. 2014.

[15] F. Parment, A. Ghiotto, T.-P. Vuong, J.-M. Duchamp, and K. Wu, "Air-filled substrate integrated waveguide for low-loss and high power-handling millimeter-wave substrate integrated circuits," *IEEE Trans. Microw. Theory Techn.*, Vol. 63, No. 4, pp. 16228–1238, Apr. 2015.

[16] I. S. S. Lima, F. Parment, A. Ghiotto, T.-P. Vuong, and K. Wu, "Broadband dielectric-to-half-mode air-filled substrate integrated waveguide transition," *IEEE Microw. Wireless Compon. Lett.*, Vol. 26, No. 6, pp. 383–385, 2016.

[17] F. Bigelli, D. Mencarelli, M. Farina, G. Venanzoni, P. Scalmati, C. Renghini, and A. Morini, "Design and fabrication of a dielectricless substrate-integrated waveguide," *IEEE Trans. Compon., Packag., Manuf. Technol.*, Vol. 6, No. 2, pp. 256–261, Feb. 2016.

[18] A. Belenguer, H. Esteban, and V. E. Boria, "Novel empty substrate integrated waveguide for high-performance microwave integrated circuits," *IEEE Trans. Microw. Theory Techn.*, Vol. 62, No. 4, pp. 832–839, Apr. 2014.

[19] A. Coves, G. Torregrosa-Penalva, A. A. San-Blas, M.A. Sánchez-Soriano, A. Martellosio, E. Bronchalo, and M. Bozzi, "A novel band-pass filter based on a periodically drilled SIW structure," *Radio Sci.*, Vol. 51, No. 7, pp. 328–336, Mar. 2016.

[20] L. Silvestri, E. Massoni, C. Tomassoni, A. Coves, M. Bozzi, and L. Perregrini, "Substrate Integrated Waveguide filters based on a dielectric layer with periodic perforations," *IEEE Trans. Microw. Theory Techn.,* Vol. 65, No. 8, pp. 2687-2697, Aug. 2017.

[21] F. Parment, A. Ghiotto, T. P. Vuong, J.M. Duchamp, and K. Wu, "Lowloss air-filled substrate integrated waveguide (SIW) band-pass filter with inductive posts," in *Proc. Eur. Microw. Conf. (EuMC)*, Paris, France, Sep. 2015, pp. 761–764.

[22] J. A. Martinez, J. J. de Dios, A. Belenguer, H. Esteban, and V. E. Boria, "Integration of a very high quality factor filter in empty substrate integrated waveguide at Q-band," *IEEE Microw. Wireless Comp. Lett.*, Vol. 28, No. 6, pp. 503–505, Jun. 2018.

[23] A. Belenguer, M. D. Fernandez, J. A. Ballesteros, J. J. de Dios, H. Esteban, and V. E. Boria, "Compact multilayer filter in empty substrate integrated waveguide with transmission zeros," *IEEE Trans. Microw. Theory Techn.*, Vol. 66, No. 6, pp. 2993–3000, Jun. 2018.

[24] J. R. Sánchez, C. Bachiller, M. Julia, V. Nova, H. Esteban, and V. E. Boria, "Microwave filter based on substrate integrated waveguide with alternating dielectric line sections," *IEEE Microw. Wireless Compon. Lett.*, Vol. 28, No. 11, pp. 990–992, Nov. 2018.

[25] C. Máximo, J. Hinojosa and A. Álvarez, "Narrowband and wideband bandpass filters based on empty Substrate Integrated Waveguide loaded with dielectric elements," *IEEE Access*, Vol. 9, pp. 32094-32105, 2021.

[26] J. Martínez, A. Coves, E. Bronchalo, A. A. San Blas and M. Bozzi, "Band-pass filters based on periodic structures in SIW technology," *AEU - Int. J. Electron. Commun.*, Vol. 112, p. 152942, 2019.

[27] J. Martínez, A. Coves, F. Mesa, and O. Quevedo-Teruel, "Passband broadening of sub-wavelength resonator-based glide-symmetric SIW filters," *AEU - Int. J. Electron. Commun.*, Vol. 125, p. 153362, 2020.

[28] A. Coves , A. A. San Blas, and E. Bronchalo, "Analysis of the dispersion characteristics in periodic Substrate Integrated Waveguides," *AEU - Int. J. Electron. Commun.*, Vol. 139, p. 153914, 2021.

[29] Robert E. Collin, "Field Theory of Guided Waves," *Wiley-IEEE Press*, 1990.

[30] ANSYS High Frequency Structure Simulator (HFSS). Available online: https://www.ansys.com/products/ electronics/ansys-hfss (accessed on March 2023).

[31] A. Coves, S. Marini, B. Gimeno, and V. Boria, "Full-wave analysis of periodic dielectric frequency-selective surfaces under plane wave excitation," *IEEE Trans Antennas and Propagation*, Vol. 60, No. 6, pp. 2760–2769, Jun. 2012.

[32] F. Bongard, J. Perruisseau-Carrier, and J. R. Mosig, "Enhanced periodic structure analysis based on a multiconductor transmission line model and application to metamaterials," *IEEE Trans. Microw.Theory Techn.*, Vol. 57, No. 11, pp. 2715–2726, Nov. 2009.

[33] S. Marini, A. Coves, V. Boria, and B. Gimeno, "Efficient modal analysis of periodic structures loaded with arbitrarily shaped waveguides," *IEEE Trans. Microw.Theory Techn.*, Vol. 58, No. 3, pp. 529–536, Feb. 2009.

[34] L. Tsang, T. H. Liao, and S. Tan, "A Fast Computation Method of Bands and Band Field Solutions of 3D Periodic Structures Using Broadband Green's Function-Multiple Scattering Theory," *Progress In Electromagnetics Research*, Vol. 176, pp. 67–93, 2023.

[35] F. Mesa, R. Rodriguez-Berral, and F. Medina, "On the computation of the dispersion diagram of symmetric one-dimensionally periodic structures," *Symmetry*, Vol. 10, No. 8, p. 307, Jul. 2018.

RAÚL GARCÍA was born in Alicante, Spain. He obtained a Bachelor's Degree in Engineering in Telecommunication Technologies, in 2021, and the Master in Telecommunication Engineering, in 2023, both at the Miguel Hernández University of Elche, Spain.

Currently, he has started his doctoral thesis in the PhD Program in Industrial and Telecommunication Technologies at Miguel Hernández University. His research interests include the analysis and design of passive waveguide components for satellite communication systems.

ÁNGELA COVES (S'04–M'05-SM'19) received the Licenciado and Ph.D. degrees in Physics from University of Valencia, Spain, in 1999 and 2004, respectively.

She is currently a Professor with the Department of Communications Engineering at Universidad Miguel Hernández de Elche, Spain. Her research interests include microwave passive components, RF breakdown high-power effects, and waveguide theory.

DARÍO HERRAIZ received his degree in telecommunications engineering from the Universidad de Castilla-La Mancha (UCLM), Spain, December 2019. He joined GAMMA group (Grupo de Aplicaciones de Microondas y Milimétricas, y Antenas) from the UCLM in 2018 for six months with a research grant, then, in 2019 as researcher, and again in 2021, also as a researcher. In 2022, he received his Post-Graduate degree in telecommunications engineering in UCLM, where he is currently pursuing the Ph.D. degree in telecommunications engineering.

His final degree project is about ESIW and was prized in 2020 with a national prize from the COITT/AEGITT (Colegio Oficial/Asociación de Graduados E Ingenieros Técnicos de Telecomunicación). So far, he has been co-author of six articles, author of one book chapter and one paper.

ÁNGEL ANTONIO SAN-BLAS received the Ingeniero de Telecomunicación and the Doctor Ingeniero de Telecomunicación degrees from the Universitat Politècnica de València, Valencia, Spain, in 2000 and 2008, respectively.

Since 2003, he has been an Associate Professor with the Departamento de Ingeniería de Comunicaciones, Universidad Miguel Hernández de Elche, Elche, Spain. His current research interests include the analysis and design of passive microwave components for communication systems.

MAURIZIO BOZZI (Fellow, IEEE) received the Ph.D. degree in electronics and computer science from the University of Pavia, Pavia, Italy, in 2000. Currently, he is a full professor of electromagnetic fields at the University of Pavia. His main research interests concern the computational electromagnetics, the substrate integrated waveguide technology, and the use of novel materials and fabrication technologies for microwave circuits.

Prof. Bozzi is the 2023 President Elect of the IEEE Microwave Theory and Technology Society (MTT-S).